WALLABY pre-pilot survey: ultra-diffuse galaxies in the Eridanus supergroup

B.-Q. For [1,2]★ K. Spekkens,[3]★ L. Staveley-Smith [1,2]★ K. Bekki,[1] A. Karunakaran [4] B. Catinella [1,2] B. S. Koribalski [5,6] K. Lee-Waddell [1,7,8] J. P. Madrid,[9] C. Murugeshan,[2,7] J. Rhee,[1,2] T. Westmeier [1,2] O. I. Wong [1,2,7] D. Zaritsky [10] and R. Donnerstein[10]

[1]*International Centre for Radio Astronomy Research, University of Western Australia, 35 Stirling Highway, Crawley, WA 6009, Australia*
[2]*ARC Centre of Excellence for All Sky Astrophysics in 3 Dimensions (ASTRO 3D)*
[3]*Royal Military College of Canada, PO Box 17000, Station Forces, Kingston, ON K7K7B4, Canada*
[4]*Instituto de Astrofísica de Andalucía, CSIC, Glorieta de la Astronomía, E-18080 Granada, Spain*
[5]*CSIRO Space & Astronomy, PO Box 76, Epping, NSW 1710, Australia*
[6]*School of Science, Western Sydney University, Locked Bag 1797, Penrith, NSW 2751, Australia*
[7]*CSIRO Space & Astronomy, PO Box 1130, Bentley, WA 6102, Australia*
[8]*International Centre for Radio Astronomy Research, Curtin University, Bentley, WA 6102, Australia*
[9]*Department of Physics and Astronomy, The University of Texas Rio Grande Valley, Brownsville, TX 78520, USA*
[10]*Steward Observatory and Department of Astronomy, University of Arizona, 933 North Cherry Avenue, Tucson, AZ 85719, USA*

ABSTRACT

We present a pilot study of the atomic neutral hydrogen gas (H I) content of ultra-diffuse galaxy (UDG) candidates. In this paper, we use the pre-pilot Eridanus field data from the Widefield ASKAP *L*-band Legacy All-sky Blind Survey to search for H I in UDG candidates found in the Systematically Measuring Ultra-diffuse Galaxies survey (SMUDGes). We narrow down to 78 SMUDGes UDG candidates within the maximum radial extents of the Eridanus subgroups for this study. Most SMUDGes UDGs candidates in this study have effective radii smaller than 1.5 kpc and thus fail to meet the defining size threshold. We only find one H I detection, which we classify as a low-surface-brightness dwarf. Six putative UDGs are H I-free. We show the overall distribution of SMUDGes UDG candidates on the size–luminosity relation and compare them with low-mass dwarfs on the atomic gas fraction versus stellar mass scaling relation. There is no correlation between gas-richness and colour indicating that colour is not the sole parameter determining their H I content. The evolutionary paths that drive galaxy morphological changes and UDG formation channels are likely the additional factors to affect the H I content of putative UDGs. The actual numbers of UDGs for the Eridanus and NGC 1332 subgroups are consistent with the predicted abundance of UDGs and the halo virial mass relation, except for the NGC 1407 subgroup, which has a smaller number of UDGs than the predicted number. Different group environments suggest that these putative UDGs are likely formed via the satellite accretion scenario.

Key words: galaxies: formation – galaxies: groups: general – galaxies: ISM.

1 INTRODUCTION

Low-surface-brightness (LSB) galaxies have been studied for decades (e.g. Impey, Bothun & Malin 1988; Bothun, Impey & Malin 1991; Dalcanton et al. 1997). With the advancement of optical imaging instruments and search techniques, a large population of extreme LSB galaxies has been uncovered (e.g. Abraham & van Dokkum 2014; Zaritsky et al. 2019). Among them, the discovery of tens to hundreds of spatially extended extreme LSB galaxies in the Coma cluster has reinvigorated the interest in studying these objects among observers and theorists (Koda et al. 2015; van Dokkum et al. 2015). These so-called ultra-diffuse galaxies (UDGs) are typically defined to have an effective radius (r_{eff}) $\geq$ 1.5 kpc and a central *g*-

band surface brightness ($\mu_{0,g}$) $\geq$ 24 mag arcsec^{-2} (van Dokkum et al. 2015). Given that this definition is mostly motivated by observational constraints, some studies suggest that UDGs may be a subclass of the LSB dwarf population (Conselice 2018; Habas et al. 2020; Lee, Hodges-Kluck & Gallo 2020a; Marleau et al. 2021). As they represent an extreme end of the LSB dwarf population, they are important in testing galaxy formation models (Boylan-Kolchin, Bullock & Kaplinghat 2012; Sawala et al. 2016).

UDGs are prevalent across all environments. They have been found in clusters (Coma cluster, e.g. Koda et al. 2015; van Dokkum et al. 2015; Yagi et al. 2016; Virgo cluster, e.g. Mihos et al. 2015; Junais et al. 2022; Hydra cluster, e.g. Iodice et al. 2020; and other clusters, see Lee et al. 2020b and references therein); in galaxy groups [Hickson Compact groups (HCGs; e.g. Román & Trujillo 2017b; Shi et al. 2017; NGC 5485 group, Merritt et al. 2016)], and in the field (e.g. Prole et al. 2019, 2021). Their physical properties also vary across environments. For example, they are generally red

★ E-mail: biqing.for@uwa.edu.au (BF); kristine.spekkens@gmail.com (KS); lister.staveley-smith@uwa.edu.au (LS)

(quiescent), smooth, and gas-poor in dense environments but blue (star-forming), irregular, and gas-rich in low-density environments (Román & Trujillo 2017b; Kadowaki et al. 2021). Their dark matter (DM) content has also sparked an intense debate about their nature and formation mechanisms. Observational evidences suggest that some of them are embedded in dwarf-sized DM haloes (Beasley & Trujillo 2016; Chilingarian et al. 2019) and in more massive DM haloes (van Dokkum et al. 2015; Zaritsky 2017; Forbes et al. 2020). Some UDGs also exhibit peculiar properties, such as high DM fractions (Beasley et al. 2016) and an offset from the established baryonic Tully–Fisher relation (Karunakaran et al. 2020; Mancera Piña et al. 2020). These pecularities challenge galaxy formation models. It is unclear if the offset from the baryonic Tully–Fisher relation is real or the result of difficulties in measuring reliable inclinations, hence rotational velocities. It is also unclear how gas-rich blue UDGs form in low-density environments and how they relate to the cluster UDGs, which tend to be gas-poor.

Several hypotheses have been proposed to form UDGs. There are two main categories which are driven by internal and external processes.

Internal processes:

(i) UDGs that are formed in dwarf-sized haloes might have higher than average spin parameters. The higher specific angular momentum of the halo prevents gas from effectively collapsing into a dense structure, which explains their extended size. In this scenario, field UDGs are predicted to be gas-rich (Amorisco & Loeb 2016; Rong et al. 2017).

(ii) In the Numerical Investigation of a Hundred Astrophysical Objects (NIHAO; Wang et al. 2015) simulation field, UDGs can be formed via repeated star formation episodes during their early evolution, which drives the gas out to larger radii. A non-negligible H I gas mass of 10^{7-9} M$_\odot$ is predicted for isolated field UDGs (Di Cintio et al. 2017). It is worth noting that UDGs may have lower star formation efficiencies than normal dwarfs despite being gas-rich (Kado-Fong et al. 2022).

External processes:

(i) UDGs may be failed $L_*(M_* \sim 10^{11}$ M$_\odot)$ galaxies that do not form stars at the rate expected for their halo mass due to star formation being quenched via ram-pressure or tidal effects (van Dokkum et al. 2015; Yozin & Bekki 2015; Martin et al. 2019; Carleton et al. 2021; Janssens et al. 2022).

(ii) Present-day UDGs are formed from excess energy and angular momentum in merging low-mass galaxies early on ($z > 1$; Wright et al. 2021).

(iii) Strong tidal interactions with larger galaxies may also form diffuse tidal dwarf galaxies that are similar to UDGs (Bennet et al. 2018; Román et al. 2021).

(iv) UDGs can be formed via tidal heating of normal dwarfs (Iodice et al. 2021; Jones et al. 2021).

While these formation mechanisms are still under debate, a wide variety of properties may suggest that they are formed via a combination of the above proposed mechanisms in different environments.

While deep optical imaging allows us to identify UDG candidates, one limitation is their distance determination. This is in part the reason that UDG searches largely associate candidates to clusters and groups at known distances. While some distances to UDGs have been obtained, sample sizes remain small due to a large amount of time that is required for spectroscopic follow-up observations (see e.g. Kadowaki, Zaritsky & Donnerstein 2017; Ruiz-Lara et al. 2018; Emsellem et al. 2019; Martín-Navarro et al. 2019; Kadowaki

et al. 2021). Observations of H I-bearing UDGs allow an easier measurement of redshifts (inferring kinematic distances), which allows clear separation of foreground dwarfs from UDGs. Such measurements also provide H I masses and linewidth/rotation velocities for disentangling the formation mechanisms. Targeted H I follow-up studies on nearby blue and star-forming UDGs have therefore been conducted and have shown to yield H I masses consistent with the theoretical prediction (Bellazzini et al. 2017; Papastergis, Adams & Romanowsky 2017; Spekkens & Karunakaran 2018; Scott et al. 2021). The untargeted Arecibo Legacy Fast ALFA (Arecibo *L*-band Feed Array) extragalactic H I survey (ALFALFA; Giovanelli et al. 2005) data have also proven to be useful in studying H I-bearing UDGs in large numbers (Leisman et al. 2017; Janowiecki et al. 2019). Recently, an H I pilot survey of optical selected UDG candidates using the Robert C. Byrd Green Bank Telescope has also been conducted (Karunakaran et al. 2020). The ongoing and previous H I studies are mostly utilizing single-dish telescopes, which have better sensitivity than interferometers, albeit at the cost of lower angular resolution.

The Widefield ASKAP *L*-Band Legacy All-sky Blind Survey (WALLABY; Koribalski et al. 2020) makes use of the large field of view of the Australian Square Kilometre Array Pathfinder (ASKAP; Johnston et al. 2007; Hotan et al. 2021) to image H I galaxies out to a redshift $z \sim 0.1$ and to cover most of the Southern hemisphere. With the survey's high angular resolution of 30 arcsec and root-mean-square (RMS) sensitivity of 1.6 mJy per beam per 18.5 kHz channel, WALLABY early science studies have been able to recover many gas-rich low-mass dwarf galaxies (see e.g. For et al. 2019, 2021; Kleiner et al. 2019). These galaxies were not resolved as individual sources in previous single-dish surveys, such as the H I Parkes All-Sky Survey (Barnes et al. 2001). WALLABY will be the first southern H I survey to provide a large number of H I redshifts and physical parameters for those H I-bearing UDGs that are identified as candidates in the DESI Legacy Imaging Surveys (Dey et al. 2019). This will allow us to investigate the proposed formation mechanisms from the H I perspective across environments.

1.1 Eridanus supergroup

The concentration of galaxies in the region of Eridanus constellation was first noted by Baker (1933). A later study by de Vaucouleurs (1975) found that Group 31 and galaxies around the NGC 1332 and NGC 1209 formed the 'Eridanus Cloud'. This cloud lies on the Eridanus–Fornax–Dorado filamentary structure and is extended to the south and in front of the 'Great Wall' ($\sim$4000 km s^{-1}; da Costa et al. 1988; Willmer et al. 1989). Its structural complexity has drawn some debate regarding its nature. Willmer et al. (1989) described it as a cluster made up of three or four subclumps. On the other hand, Omar & Dwarakanath (2005) considered that the galaxies in the region as loose groups and form an intermediate evolutionary stage between the Ursa-Major group and the Fornax cluster. Brough et al. (2006) reanalysed this region using the 6dF Galaxy Survey (6dFGS; Jones et al. 2004) and concluded that this region is occupied by three distinct groups, namely the NGC 1407 ($v = 1658 \pm 26$ km s^{-1}), NGC 1332 ($v = 1474 \pm 18$ km s^{-1}), and Eridanus ($v = 1638 \pm 5$ km s^{-1}) groups. These groups also form part of the supergroup, which is defined as a group of groups that may eventually merge to form a cluster.

The Eridanus supergroup is an interesting system as it is on the evolutionary path to cluster assembly similarly to the Ursa-Major supergroup (Wolfinger et al. 2016). There are only a few known supergroups in the Universe that allow us to better understand galaxy

evolutionary pathways (Tran et al. 2009). Galaxies in the Eridanus supergroup are more H I-deficient as compared to galaxies in the Ursa-Major supergroup and in the field (For et al. 2021; Murugeshan et al. 2021). There are two enormous H I clouds in the Eridanus supergroup without optical counterparts (Wong et al. 2021), and the importance of tidal interactions in the Eridanus supergroup has been recently demonstrated (Wang et al. 2022).

In this paper, we present a pilot study of H I content of optically identified UDG candidates in the WALLABY pre-pilot Eridanus field and discuss implications for their formation mechanisms. This paper is structured as follows. Section 2 describes the selection criteria of UDG candidates, the methodology used to search for H I, and the derivation of their physical parameters. In Section 3, we perform the analysis of their distribution with respect to the low-mass dwarf population on the atomic gas fraction versus stellar mass scaling relation, the predicted number of UDGs based on the virial masses of the host system, tidal or ram-pressure stripping as a possible formation channel, gas-richness as compared to other UDGs in group and cluster environments. We summarize our findings and discuss future work in Section 4.

Throughout the paper, we adopt a Lambda cold dark matter (ΛCDM) cosmology model with $\Omega_M = 0.27$, $\Omega_K = 0$, $\Omega_\Lambda = 0.73$, and $H_0 = 73$ km s^{-1} Mpc^{-1}. These are the default parameters for distances and cosmologically corrected quantities in the NASA/IPAC Extragalactic database (Spergel et al. 2007).

2 UDG CANDIDATES

We select the UDG candidates from the third Systematically Measuring Ultra-diffuse Galaxies survey (SMUDGes) catalogue (Zaritsky et al. 2022). This catalogue focuses on identifying UDG candidates from the southern portion of the ninth data release (DR9) of the DESI Legacy Imaging Surveys (Dey et al. 2019). The classification is performed using a modified version of a deep learning model with visual confirmation. Objects with LSB ($\mu_{0,g} \geq 24$ mag arcsec^{-2}) and large angular extent (effective radii; $r_{eff} \gtrsim 5.3$ arcsec, which corresponds to $r_{eff} \geq 2.5$ kpc at the distance of the Coma cluster), are set as the main selection criteria for the imaging data search in SMUDGes. We refer the reader to a detailed description of the image processing and the automated method for identifying the UDG candidates in Zaritsky et al. (2019, 2021).

In Fig. 1, we show the distribution of SMUDGes UDG candidates within a $10° \times 10°$ area of the Eridanus supergroup (crosses). The maximum radial extent of the Eridanus, NGC 1407, and NGC 1332 groups (Brough et al. 2006) are represented as black circles. The ASKAP observed area is marked with the dashed diamond, which fully covers the Eridanus group. The red circles represent the H I detections in For et al. (2021), hereafter F21. The H I sources in F21 generally have a higher optical surface brightness than the SMUDGes UDG candidates. There are 97 and 78 SMUDGes UDG candidates within the WALLABY pre-pilot footprint and within the maximum radial extents of the groups that comprise the Eridanus supergroup, respectively.

The completeness of the SMUDGes catalogue is estimated to be a better representation of the population of large ($r_{eff} > 2.5$ kpc) UDGs beyond $cz \sim 1800$ km s^{-1}. Given that the distance to the Eridanus supergroup is about 1/5 (one-fifth) of the distance to Coma (100 Mpc), the vast majority of SMUDGes UDG candidates in this region are likely not true UDGs. A spatial variation of SMUDGes UDG candidates is seen in the Eridanus field. Examining the observed footprints of Dark Energy Camera Legacy Survey (DECaLS) of this field, we find only minor differences in depth. Excluding faint
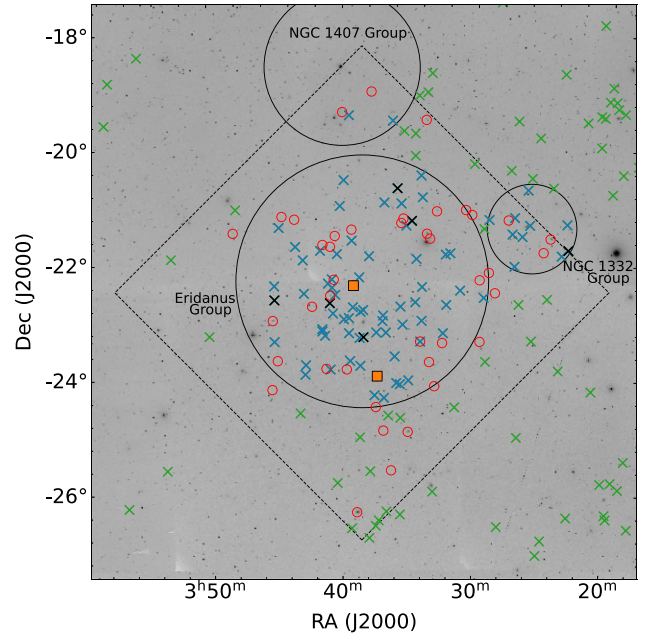
Figure 1. UDG candidates in the Eridanus field (crosses) from the SMUDGes 3rd catalogue overlaid on to an optical Digital Sky Survey (DSS-2) *r*-band image. The maximum radial extent of Eridanus (0.8 Mpc), NGC 1332 (0.3 Mpc), and NGC 1407 (0.5 Mpc) are marked as black circles. UDG candidates within the maximum radial extents and selected for this study are shown as the blue crosses. Those UDG candidates that fall outside the maximum radial extent but within the Eridanus field are shown as the green crosses. Those identified as putative UDGs ($r_{eff} > 1.5$ kpc at an assumed distance of 21 Mpc) are shown as the black crosses (see Section 2.2). The WALLABY footprint is $\sim 6° \times 6°$, which is shown as the dashed diamond. The red circles and orange squares represent the H I detections and the H I clouds in For et al. (2021), respectively.

candidates does not change the spatial variation that we see in the field.

2.1 Searching for H I

To search for H I in the SMUDGes UDG candidates, we extract a subcube at the position of each SMUDGes UDG candidate from the WALLABY mosaicked cube of the Eridanus field. We extract the subcubes using three velocity ranges (~ 680–2500, ~ 2000–7000, and ~ 7000–13 000 km s^{-1}), which resulted in 97 $\times$ 3 subcubes. Each subcube covers $0.1° \times 0.1°$ in area. The first velocity range covers the Eridanus supergroup.

We run the Source Finding Application (SOFIA[1]; Serra et al. 2015; Westmeier et al. 2021) to search for H I using 3.0σ, 3.5σ, 4.0σ, 4.5σ, and 5.0σ detection thresholds. We note that sources presented in the F21 catalogue are detected with a 5.0σ threshold, where the local RMS is calculated from a larger area and a wider velocity range than each extracted subcube. It is possible that changes of local RMS and lower thresholds might yield H I detections that fall below the 5σ detection threshold. Subsequently, we check the reliability plots from SOFIA, and all detections by eye using Hanning-smoothed cubes and DR9 DESI Legacy Imaging Survey images. We only find one reliable H I detection, which is also known as WALLABY J033408−232125 ($cz = 1262$ km s^{-1}) in the F21 catalogue. This H I detection is also a

---

[1] Available at https://github.com/SoFiA-Admin/SoFiA-2/.

member of the Eridanus group (see F21). As a result of not finding any H I detection outside the maximum radial extents of these groups that make up the Eridanus supergroup (but still within WALLABY observed footprints), we will focus on analysing the 78 SMUDGes UDG candidates that are within the maximum radial extents of these groups for the rest of the paper. We note that there are two SMUDGes UDG candidates in the NGC 1332 group that fall outside of the ASKAP field of view. The search algorithm of SMUDGes also does not detect any UDG candidates within 2 arcmin of the enormous H I clouds in the Eridanus group (Wong et al. 2021).

2.2 Properties and physical parameters of SMUDGes UDG candidates

Assuming that these 78 SMUDGes UDG candidates are group members of the Eridanus subgroups, we adopt a luminosity distance of $D_L = 21$ Mpc (see section 5 of F21) to calculate their r_{eff}. To obtain the stellar masses, we employ the mass-to-light ratio (M/L) relation in Zibetti, Charlot & Rix (2009)[2] as follows:

$$\log(M_*/M_\odot) = -0.804 + 1.654(g - r) + \log(L_r/L_\odot), \quad (1)$$

where $g - r$ is an extinction-corrected colour and L_r is the r-band luminosity measured from the DR9 Dark Energy Spectroscopic Instrument (DESI) Legacy Survey images. The absolute magnitude of the Sun ($M_{Sun,abs}$) in different Dark Energy Survey (DES) wavebands is given in Willmer (2018). The r-band absolute magnitude is given as $M_{r,abs} = r - 5\log(D_L) + 5 - A_r$, where D_L is the luminosity distance in pc. We adopt the A_r (extinction) value in the r-band used for the SMUDGes catalogue (Zaritsky et al. 2022). In Fig. 2, we show the distributions of r_{eff}, M_*, and $g - r$ for our SMUDGes UDG candidates.

The definition of UDGs varies significantly in the literature. The widely accepted definition, i.e. $r_{eff} \geq 1.5$ kpc and $\mu_{0,g} \geq 24$ mag arcsec^{-2}, stems from the samples in van Dokkum et al. (2015). There is a wide range of parameters being explored as selection criteria by various studies. For example, Yagi et al. (2016) and Román & Trujillo (2017b) use $r_{eff} > 0.7$ kpc and $r_{eff} > 1.3$ kpc as their minimum radius definition, respectively. This is solely motivated by observational constraints rather than a physical reason. There are other constraints which have variously been suggested, such as stellar mass, absolute magnitude, and/or luminosity, to explicitly limit UDGs to dwarf mass populations (see Mihos et al. 2015; Iodice et al. 2020; Lim et al. 2020).

In this paper, we consider putative UDGs to have $r_{eff} > 1.5$ kpc. This allows us to make a direct comparison with previous studies. With this definition, we obtain six putative UDGs among our 78 SMUDGes UDG candidates, with five and one belonging to the Eridanus and NGC 1332 groups, respectively. WAL-LABY J033408−232125 has $r_{eff} > 1.1$ kpc and hence will be considered as an LSB dwarf rather than a UDG in this work.[3] In Fig. 3, we overplot our SMUDGes UDG candidates (LSB dwarfs + putative UDGs) on to the size–luminosity relation of dwarf galaxy populations (grey dots) compiled by Brodie et al. (2011)[4] and the central dwarf galaxy population in the Next Generation Fornax Survey (NGFS;
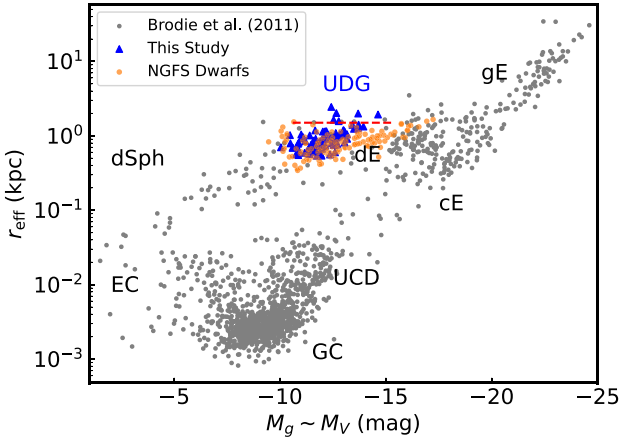
[2]An initial mass function of Chabrier (2003) is adopted.
[3]Note that if we were to consider the definition of $r_{eff} > 1.0$ kpc from the theoretical NIHAO simulation, the total number of putative UDGs would increase to 22 and WALLABY J033408−232125 would be considered as a UDG instead based on its redshift.
[4]https://sages.ucolick.org/spectral_database.html
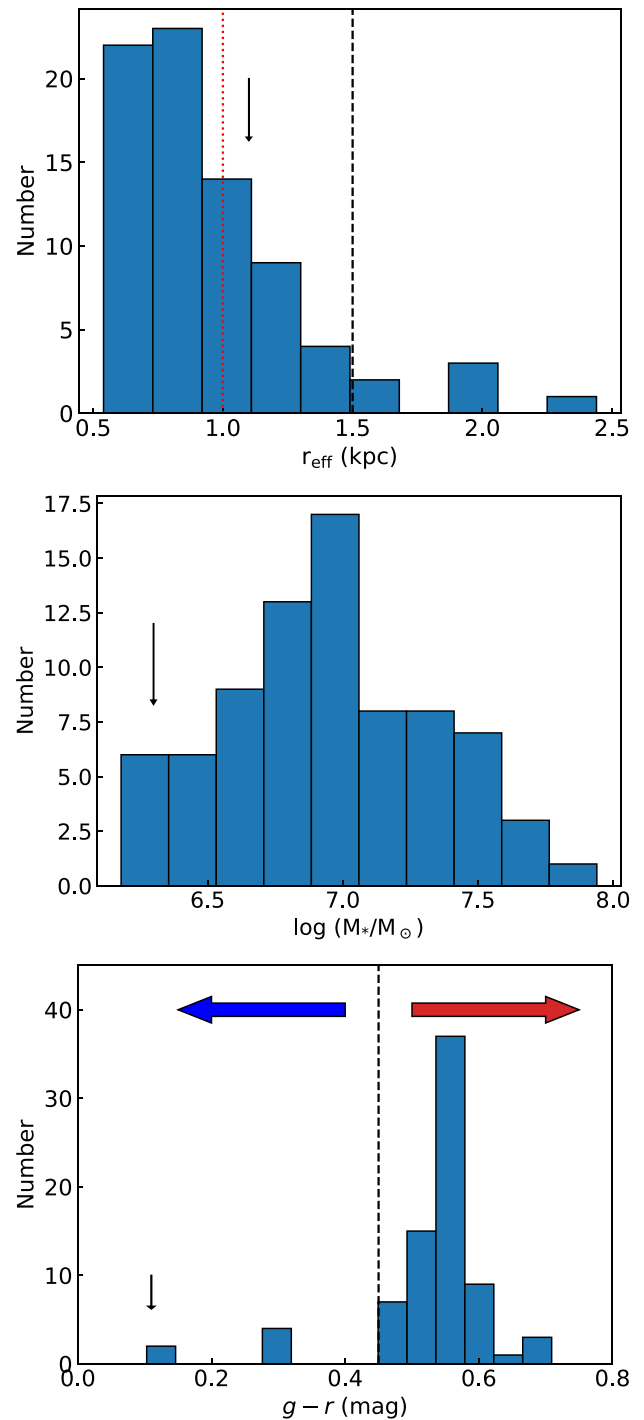
Figure 2. Histograms of r_{eff} in kpc at an assumed distance of 21 Mpc (top), $\log(M_*/M_\odot)$ (middle), and $g - r$ colour in magnitude (bottom) for 78 SMUDGes UDG candidates that are within the maximum radial extents of the Eridanus subgroups. Bias corrections (if applicable) have been applied to r_{eff} and colour as given in Zaritsky et al. (2022). The black arrow indicates the position of the H I detected source. Top: The dashed and dotted lines at 1.5 and 1.0 kpc represent the boundaries of the defined observation and simulations UDG effective radius, respectively. Bottom: The dashed line at $g - r = +0.45$ mag represents the boundary of the defined red and blue colour for the SMUDGes UDG candidates. The definition is based on the joint distribution of colour ($g - r$) and Sérsic index (n) with the tail of red objects with $n > 1$ and $g - r > +0.45$ mag (Zaritsky et al. 2021) (see Table 1).

Figure 3. Size–luminosity relation of dwarf galaxy populations. Grey dots, blue triangles, and orange dots represent objects compiled by Brodie et al. (2011), this study, and NGFS dwarfs (Eigenthaler et al. 2018), respectively. Size is represented by effective radius (r_{eff}) in kpc with SMUDGes UDG candidates (LSB dwarfs + putative UDGs) at an assumed distance of 21 Mpc. The red dashed line indicates $r_{\text{eff}} = 1.5$ kpc. Absolute magnitudes in the DES g band (extinction corrected) are used for our SMUDGes UDG candidates (LSB dwarfs + putative UDGs) sample, which is equivalent to the absolute V-band magnitude in Brodie et al. (2011). dSph: dwarf Spheroidal; dE: dwarf Elliptical; gE: giant Elliptical; cE: compact Elliptical; UCD: Ultra Compact Dwarf; GC: Globular Cluster; EC: very faint, Extended Cluster; UDG: Ultra-Diffuse Galaxy.

Eigenthaler et al. 2018). Brodie et al. (2011) samples are limited to objects that have confirmed distances either by spectroscopy, resolved stellar populations, or surface brightness fluctuations. Our SMUDGes UDG candidates (LSB dwarfs + putative UDGs) sample extends to the fainter end of the dwarf Spheroidal (dSph) galaxies. The NGFS dwarf galaxy population (nucleated and non-nucleated) overlaps with the UDGs parameter space and is extended toward the brighter end of the dwarf Elliptical (dE). This has drawn some debate if UDGs are at the large end of the dwarf locus or are branching out into its own sequence. They are generally low-mass ($M_* < 10^8\ \text{M}_\odot$) and the majority of them are fairly red in colour ($g - r > 0.45$ as defined in Zaritsky et al. 2021). The median Sérsic index (n) is ~0.8 in the SMUDGes catalogue. This value is consistent with theoretical predictions (Jiang et al. 2019).

For non-H I detections, we calculate their upper H I mass limit ($z \sim 0$) as follows:

$$M_{\text{H I,lim}} = 236 \times 10^3 \times S_{\text{int}} \times D_{\text{L}}^2, \qquad (2)$$

where $S_{\text{int}} = 5\sigma \times \Delta v$ is the H I integrated flux, in Jy km s^{-1} and D_{L} is the luminosity distance of 21 Mpc. We adopt a fiducial velocity width (Δv) of 30 km s^{-1} (see e.g. Jones et al. 2021). 1σ noise level is calculated from 100 source free channels of each subcube that covers the velocity range of 680–2500 km s^{-1}. We summarize the properties and physical parameters of our SMUDGes UDG candidates (LSB dwarfs + putative UDGs) sample in Table 1.

3 ANALYSIS

3.1 Atomic gas fraction–stellar mass scaling relation

The atomic gas fraction ($M_{\text{H I}}/M_*$) versus stellar mass (M_*) scaling relation allows us to understand the physical processes that regulate the conversion of gas into stars and drive the changes in galaxy

morphology (see e.g. Janowiecki et al. 2017; Saintonge & Catinella 2022).

The Extended *GALEX* Arecibo SDSS Survey (xGASS; Catinella et al. 2018) investigates this relation for a representative sample of ~1200 galaxies, selected from the SDSS DR7 (Abazajian et al. 2009) by stellar mass and redshift only ($9.0 < \log(M_*/\text{M}_\odot) < 11.5$ and $0.01 < z < 0.05$), and observed down to a gas fraction limit of 2–10 per cent, depending on M_*. Its stellar mass selected H I sample shows a clear linear relation of increasing $\log(M_{\text{H I}}/M_*)$ with decreasing $\log(M_*/\text{M}_\odot)$, but it is unclear if the trend continues to rise below the $\log(M_*/\text{M}_\odot) = 9.0$ limit of the survey. Using the ALFALFA.40 sample with stellar masses derived from SDSS spectra and photometry, Maddox et al. (2015) show that the gas fraction follows the same trend as in the xGASS sample at higher stellar mass ($M_* > 10^9\ \text{M}_\odot$) but flattens out at the lower stellar mass end indicating a higher gas content in the low-mass regime.

To further investigate the trend in the low-mass regime, F21 compare various low-mass dwarf samples with the Maddox et al. (2015) empirical relations (see fig. 12 of F21). It is evident that the sub-sample of gas-rich local volume dwarfs selected from ALFALFA.40 in Huang et al. (2012) does not show the flattening trend as seen in Maddox et al. (2015). In Huang et al's sub-sample, the atomic gas fraction continues to rise with decreasing M_*. This is due to stellar masses in the ALFALFA.40 sample being underestimated for low-mass galaxies, which is a known issue with the SDSS reduction pipeline (Huang et al. 2012). The derived stellar masses via the spectral energy distribution fitting method in Huang et al. (2012) are higher by comparison. F21 show that the sample from the Survey of H I in Extremely Low-mass Dwarfs (SHIELD; McQuinn et al. 2021) also supports a non-flattening trend in the low-mass regime. The SHIELD sample mostly consists of isolated dwarf galaxies. It is unclear if the low-mass dwarf population in the Eridanus supergroup follows such a trend due to a lack of low-mass ($<10^8\ \text{M}_\odot$) galaxies in F21.

With a large number of low-mass galaxies in this study, we revisit the atomic gas fraction scaling relation in the low-mass regime of the Eridanus supergroup. In Fig. 4, we show the distribution of the ALFALFA.40 sub-sample (blue crosses; Huang et al. 2012), the SHIELD sample (red triangles; McQuinn et al. 2021), the Eridanus supergroup sample (orange circles; F21), the Leo T dwarf galaxy (green cross; Adams & Oosterloo 2018), and our SMUDGes UDG candidates (LSB dwarfs + putative UDGs) sample (grey points) on the atomic gas fraction scaling relation. The atomic gas fraction values for our SMUDGes UDG candidates (LSB dwarfs + putative UDGs) sample are set to be their upper limit with the exception of one H I detected LSB dwarf (see Section 2.1). The dashed line is adopted from F21 and is for guidance only. Our sample falls along the WALLABY sensitivity limit line, which also lies within the scatter of the gas-rich dwarf population. We note that galaxies in the Eridanus supergroup are generally more H I-deficient as compared to galaxies in other galaxy groups (see e.g. For et al. 2019). Nevertheless, the finding of a non-flattening trend based on ALFALFA.40 sub-sample and SHIELD sample in the low-mass regime suggests that low-mass, high gas fraction galaxies might be rarer than expected. It is inconclusive regarding the flattening trend in the low-mass regime using our sample. It would be useful to revisit such relation in the low-mass regime with the full WALLABY survey in the future.

3.2 Gas richness

We investigate the gas richness of our SMUDGes UDG candidates (LSB dwarfs + putative UDGs) sample using distance independent

Table 1. Properties and derived parameters of SMUDGes UDG candidates (LSB dwarfs + putative UDGs).

ID	Designation	α (J2000) (deg)	δ (J2000) (deg)	$g - r$ (mag)	M_r (mag)	$\log M_*$ ($M_\odot$)	$\log M_{HI}$ ($M_\odot$)	$\log(M_{HI}/M_*)$	R_{eff} (arcsec)	R_{eff} (kpc)
(1)	(2)	(3)	(4)	(5)	(6)	(7)	(8)	(9)	(10)	(11)
				Eridanus group						
1	SMDG 0336515−242027	54.21476	−24.34079	0.555	−13.723	7.45	<7.55	<0.11	8.94	0.91
2	SMDG 0337349−241754	54.39532	−24.29840	0.501	−12.693	6.95	<7.56	<0.62	11.30	1.15
3	SMDG 0335396−240610	53.91490	−24.10278	0.504	−11.899	6.63	<7.55	<0.92	9.93	1.01
4	SMDG 0335557−240456	53.98221	−24.08214	0.592	−13.230	7.31	<7.55	<0.24	7.48	0.76
5	SMDG 0335006−240205	53.75237	−24.03474	0.555	−13.378	7.31	<7.55	<0.24	10.34	1.05
6	SMDG 0342509−235621	55.71210	−23.93930	0.577	−11.349	6.53	<7.66	<1.13	5.58	0.57
7	SMDG 0340559−235101	55.23296	−23.85031	0.519	−12.394	6.86	<7.67	<0.81	7.96	0.81
8	SMDG 0338400−234705	54.66684	−23.78466	0.562	−13.298	7.29	<7.64	<0.36	9.65	0.98
9	SMDG 0342478−234626	55.69903	−23.77390	0.570	−12.843	7.12	<7.66	<0.54	9.99	1.02
10	SMDG 0339260−234204	54.85834	−23.70116	0.569	−12.147	6.84	<7.66	<0.82	8.47	0.86
11	SMDG 0336039−233707	54.01629	−23.61862	0.549	−12.674	7.02	<7.58	<0.56	7.32	0.75
12	SMDG 0345106−232201	56.29428	−23.36689	0.536	−12.292	6.84	<7.63	<0.79	8.11	0.83
13	SMDG 0334081−232128[a]	53.53354	−23.35785	0.103	−12.733	6.30	<7.54	<1.24	10.72	1.09
14	SMDG 0338435−231802	54.68114	−23.30051	0.555	−14.235	7.65	<7.63	<−0.02	12.95	1.32
15	SMDG 0338261−231711[b]	54.60877	−23.28646	0.466	−12.999	7.01	<7.64	<0.63	16.07	1.64
16	SMDG 0341202−231539	55.33436	−23.26092	0.592	−13.117	7.27	<7.63	<0.36	7.35	0.75
17	SMDG 0339319−231306	54.88274	−23.21826	0.509	−11.983	6.68	<7.63	<0.96	7.43	0.76
18	SMDG 0332252−231233	53.10507	−23.20915	0.548	−14.487	7.74	<7.54	<−0.20	13.06	1.33
19	SMDG 0336444−231222	54.18518	−23.20610	0.538	−12.559	6.95	<7.62	<0.66	11.20	1.14
20	SMDG 0337279−231213	54.36616	−23.20352	0.554	−12.238	6.85	<7.63	<0.78	8.90	0.91
21	SMDG 0341326−231108	55.38587	−23.18560	0.537[c]	−12.198[c]	6.81	<7.62	<0.81	11.60	1.18
22	SMDG 0341331−230852	55.38812	−23.14772	0.462	−11.061	6.23	<7.61	<1.38	6.74	0.69
23	SMDG 0335286−230353	53.86915	−23.06482	0.597[c]	−11.070[c]	6.46	<7.58	<1.13	9.99	1.02

This table is available in its entirety as supporting information with the electronic version of the paper. A portion is shown here for guidance regarding its form and content.

[a]: Also known as WALLABY J033408−232125.

[b]: Putative UDG.

[c]: No bias correction due to being flagged as inaccurate (Zaritsky et al. 2022). #: Within maximum radial extent of the NGC 1332 group but outside the WALLABY observed footprints. Col (1): Identification number. Cols (2)–(4): Designation, α and δ (J2000) coordinates are based on the SMUDGes catalogue (Zaritsky et al. 2022). Col (5): Extinction and bias (if applicable) corrected $g - r$ magnitude. Col (6): Absolute magnitude in r band. Col (7): Stellar mass in logarithmic scale. Col (8): Upper limit of H I mass, with the exception of WALLABY J033408−232125, in logarithmic scale. Col (9): Atomic gas fraction. Col (10): Effective radius in arcsec, which is derived using DR9 DESI Legacy Survey stacked images of grz bands. Bias correction has been applied if applicable. Col (11): Effective radius in kpc for an assumed distance of 21 Mpc.

measurements. In Fig. 5 (top panel), we show the distribution of $\log(M_{HI}/L_g)$ versus $g - r$. The H I upper limits of our sample are represented by the arrows, with six putative UDGs in red and green for the Eridanus and NGC 1332 groups, respectively. The H I detected UDGs in the Coma cluster (blue crosses; Karunakaran et al. 2020) and our H I detected LSB dwarf (orange square) are also shown. The dashed line represents $g - r = 0.45$ that marks the blue and red colour boundary. According to Karunakaran et al. (2020), H I detected UDGs are bluer and have more irregular morphologies, while the non-H I detected UDGs are redder and smoother in morphologies. We find that the two putative UDGs (red arrows) and two LSB dwarfs (grey arrows) with $g - r < 0.45$ have a smooth morphology. While the sample is small, it is possible that different morphologies resulting from different evolutionary paths might affect the gas content of the UDGs. The majority (∼94 per cent) of putative UDGs and LSB dwarfs in this study are red in colour. This is not a surprise given that UDGs in denser environments tend to be redder (Kadowaki et al. 2021). The unusually blue colour of LSB dwarf, SMDG 0334081−232128 (also known as WALLABY J033408−232125), suggests ongoing star formation with a star formation rate estimated to be 0.0002 $M_\odot$ yr^{-1} (F21).

The bottom panel of Fig. 5 shows the distribution of atomic gas fraction $\log(M_{HI}/M_*)$ versus r_{eff} with the colour scale representing stellar mass. The triangles, squares, and circles represent the H I detected UDGs in the Coma cluster (Karunakaran et al. 2020), LSB dwarfs with and without H I in our study, respectively. A scatter of ∼1 dex is present for $r_{eff} < 1.0$ kpc. There is no obvious trend beyond $r_{eff} > 1.5$ kpc but our sample size is small. UDGs in the Coma cluster are massive by comparison to our putative UDGs. The atomic gas fraction of Coma cluster UDGs also has $\log(M_{HI}/M_*) < 1.0$ indicating that the relative gas content is lower than our sample.

3.3 Number of UDGs and virial masses of their host haloes

The number of UDGs (N_{UDG}) is known to have a power-law relation with the virial masses (M_{200}) of the host haloes, $N_{UDG} \propto M_{200}^\alpha$ (van der Burg, Muzzin & Hoekstra 2016; Janssens et al. 2017; van der Burg et al. 2017; Mancera Piña et al. 2018; Lee et al. 2020b). The power-law index, α, gives an indication of how effectively a galaxy is formed and survives its environment. If $\alpha = 1$, the number of galaxies is directly proportional to the mass of the host halo. In this case, these galaxies are not strongly affected by environmental effects. If $\alpha < 1$, galaxies in low-density environments have relatively higher number densities per unit mass of their host haloes. These galaxies are preferentially formed and survive in low-density environments (field or galaxy group). If $\alpha > 1$, these galaxies are formed more efficiently or survive longer in high-density environments (cluster; Lee et al. 2020b).
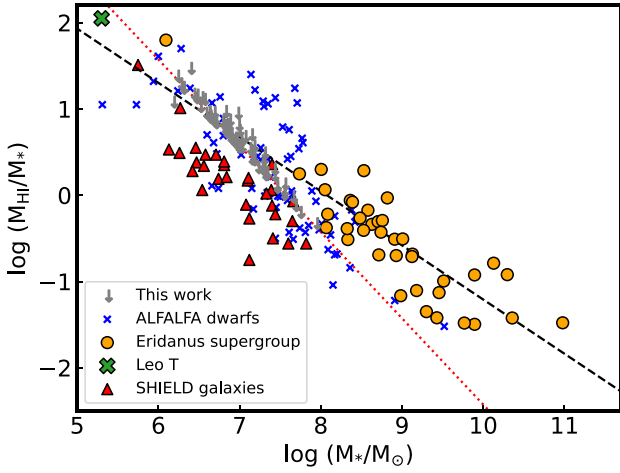
Figure 4. Atomic gas fraction ($M_{\rm H\,I}/M_*$) versus stellar mass (M_*) scaling relation in logarithmic scale. SHIELD galaxies (red triangles), dwarf galaxies from the ALFALFA.40 sub-sample (blue crosses), the Eridanus supergroup with H I detections (orange dots), SMUDGes UDG candidates (LSB dwarfs + putative UDGs) (grey arrows) with distances assumed to be equal to that of the Eridanus supergroup (non-H I detections) and Leo T (green cross) are plotted for comparison. The black dashed line is derived in F21. The red dotted line is the gas-fraction sensitivity limit (5σ) at the distance of the Eridanus supergroup (21 Mpc). 1σ is equivalent to 2.4 mJy (F21).

A list of UDG numbers and virial masses of galaxy groups and clusters has been compiled by Lee et al. (2020b) based on the same selection criteria as in this study. Lee et al. (2020b) fit the $N_{\rm UDG} \propto M_{M_{200}}^{\alpha}$ relation by considering the data points with $M_{200} > 10^{13}$ $M_\odot$, $M_{200} > 10^{12}$ $M_\odot$, and full range of M_{200}. There are fewer data points for fitting the relation on host haloes with $M_{200} < 10^{13}$ $M_\odot$ as there are fewer UDGs in low-mass haloes. Using all available data in Lee et al. (2020b), we obtain a Pearson correlation coefficient of 0.94 indicating a tight correlation. Overall, their derived α is close to 1, which suggests that the formation and survival of UDGs are less affected by the environment. However, we caution that the power-law fitting is affected by selection bias and small number statistics, especially for lower mass host haloes. This is clearly demonstrated by using the Galaxy and Mass Assembly (GAMA) group sample, where van der Burg et al. (2017) obtain $\alpha = 1.11$. Their sample is also less abundant per unit halo mass than the HCGs (Román & Trujillo 2017b). The deviation might be due to the lack of UDGs in the GAMA groups and the group properties, as loose galaxy groups are not included in the HCGs.

Recently, Karunakaran & Zaritsky (2023) study the abundance of UDGs around 75 nearby Milky Way-like systems using literature satellite galaxy catalogues. Their investigation bolsters the low halo mass end of the UDG abundance relation and finds a slope of $\alpha = 0.89$ for this relation. Crucially, they demonstrate that there are various systematics (e.g. UDG definitions, photometric completeness, and host redshifts) between various UDG abundance studies in the literature that can affect the result slopes and highlight the need for more uniform studies of this trend. Nevertheless, as explained in their work, the majority of existing slopes hover around a slope of unity and imply little to no effect of the environment on UDG abundance.

To predict the number of UDGs in the Eridanus supergroup, we apply the power-law relation (with $\alpha = 0.99$) in Lee et al. (2020b) to the halo masses of the NGC 1407 (7.9×10^{13} $M_\odot$), NGC 1332 (1.4×10^{13} $M_\odot$), and Eridanus (2.1×10^{13} $M_\odot$) groups as listed
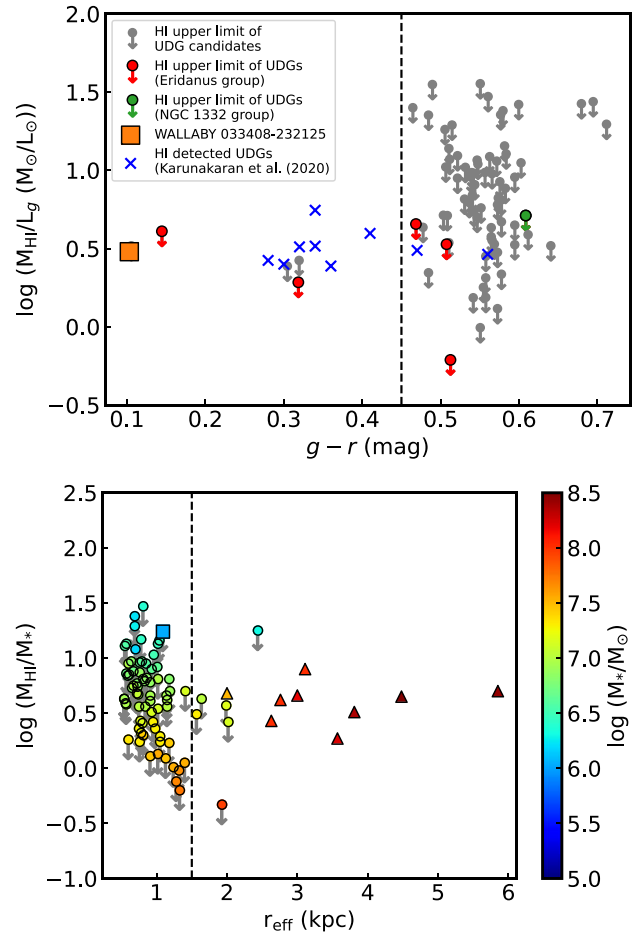
Figure 5. Top: Distribution of $\log(M_{\rm H\,I}/L_{\rm g}$ ($M_\odot/L_\odot$)) versus $g - r$. All magnitudes are extinction and bias corrected. The dashed line divides the red and blue populations at $g - r = 0.45$. The orange square and blue crosses represent the H I detected LSB dwarf in our study and H I detected UDGs in Karunakaran et al. (2020), respectively. The arrows show the upper limit of $M_{\rm H\,I}/L_{\rm g}$ for five and one putative UDGs in the Eridanus and NGC 1332 groups are shown as red and green arrows, respectively. Bottom: Distribution of $\log(M_{\rm H\,I}/M_*)$ versus $r_{\rm eff}$. Bias corrections have been applied to $r_{\rm eff}$ values. The colour scale indicates the stellar masses. The SMUDGes UDG candidates (LSB dwarfs + putative UDGs) sample in our study are represented by circles (H I non-detections) and square (H I detection). H I detected UDGs in the Coma cluster are shown as triangles (Karunakaran et al. 2020). The arrows show the upper limit of $M_{\rm H\,I}/M_*$.

in Brough et al. (2006). We obtain $N_{\rm UDG} = 3$, 5, and 17 for the NGC 1332, Eridanus, and NGC 1407 groups, respectively. Our sample yields 1^{+3}_{-1}, 5^{+8}_{-5}, and 0^{+2} putative UDGs for the NGC 1332, Eridanus, and NGC 1407 groups, respectively. The uncertainties are based on the Poisson statistics. Taking into account the uncertainties in halo masses, the predicted numbers of UDGs for the NGC 1332 and Eridanus groups are consistent with our finding (assuming the projected distance of 21 Mpc). However, the number of UDGs in the NGC 1407 group is lower than the number predicted by the power-law relation ($N_{\rm UDG} = 17 \pm 6$). This is not a surprise given that the number of SMUDGes UDG candidates in the NGC 1407 group is small to begin with (refer to Fig. 1). In Fig. 6, we show the relation between $N_{\rm UDG}$ and M_{200} for a sample of groups and clusters, including the new data. The fit suggests $\alpha = 0.99$.
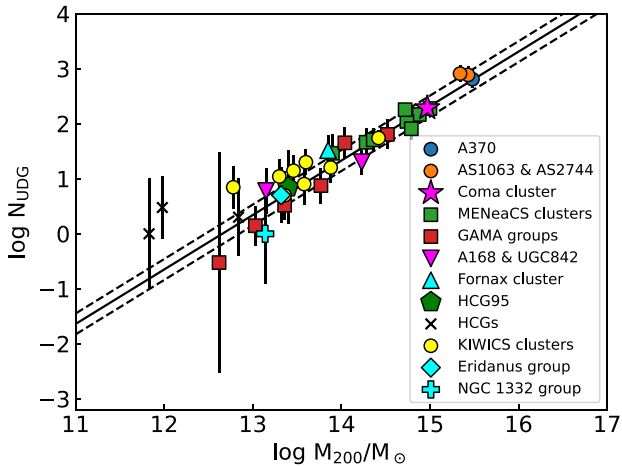
Figure 6. Number of UDGs and virial mass of their host system in logarithmic scale. The number of UDGs in other galaxy groups and clusters is compiled and listed in table 7 of Lee et al. (2020b). Blue circle: A370 (Lee et al. 2020b); orange circles: AS1063 and AS2744 (Lee et al. 2017); magenta star: Coma cluster (Yagi et al. 2016); green squares: MENeaCS clusters (van der Burg et al. 2016); red squares: GAMA groups (van der Burg et al. 2017); magenta nablas: A168 and UGC842 (Román & Trujillo 2017a); cyan triangle: Fornax cluster (Venhola et al. 2017); green pentagon: HCG95 (Shi et al. 2017); black crosses: HCGs (Román & Trujillo 2017b); yellow circles: KIWICS clusters (Mancera Piña et al. 2018); cyan diamond: Eridanus group (this study); cyan plus: NGC 1332 group (this study). The solid and dashed lines represent $\log(N_{UDG}) = 0.99 \times \log M_{200}/M_\odot - 12.53 \pm 0.67$ and RMS of 0.19 dex.

To investigate if spatial density might contribute to a higher number of SMUDGes UDG candidates in different groups, we plot the spatial projected distribution of galaxies in the region of the Eridanus supergroup (grey dots) in Fig. 7. These galaxies are extracted from the 2MASS All-Sky Extended Catalogue (XSC; Jarrett et al. 2000). Our putative UDGs and H I detected LSB dwarf are represented by green squares and a blue triangle, respectively. The non-H I detected LSB dwarfs and other SMUDGes UDG candidates in the Eridanus field are represented by red dots. We find that the density of LSB dwarfs (initially as SMUDGes UDG candidates) in the Eridanus field is at its highest in the Eridanus group as compared to the NGC 1407 and NGC 1332 groups. The projected locations of putative UDGs do not show a correlation with the density of LSB dwarfs. The slightly different environments between these groups could explain the actual number of UDGs in the groups.

The NGC 1407 group has a centroid located 16 kpc from the large elliptical galaxy NGC 1407 (Brough et al. 2006). It is the only group in the supergroup that contains X-ray emission. Due to its high mass-to-light ratio, low spiral fraction, and symmetric intragroup X-ray emission, it is considered to be virialized. The higher X-ray luminosity of the NGC 1407 group compared to other galaxy groups (Miles et al. 2004) also suggests that the NGC 1407 group is dynamically stable. While NGC 1407 group is not a cluster, the presence of X-ray emission and a large fraction of early-type galaxies suggest that its evolutionary stage is more consistent with galaxy clusters (where UDGs are gas-poor) than young galaxy groups. On the contrary, the Eridanus group is not centred on any particular galaxy. Its centroid is 300 kpc from the brightest elliptical galaxy (NGC 1395) in the group. It is a loose and dynamically young group that is yet to reach a stable stage of evolution (F21).
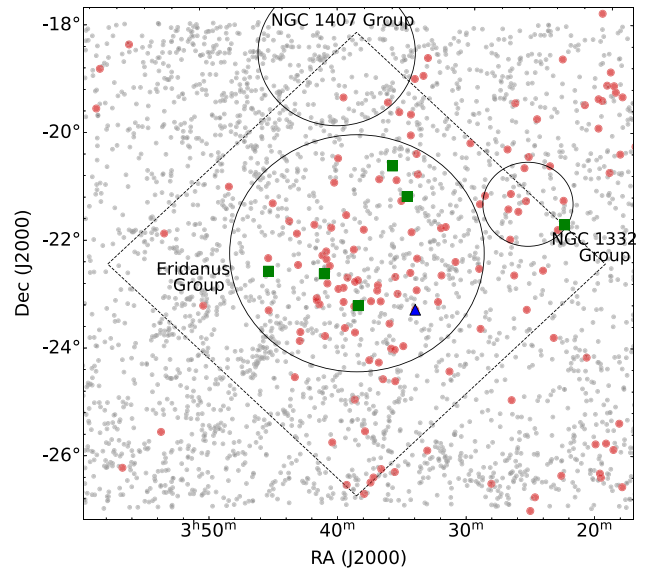

Figure 7. Spatial distribution of galaxies in the region of the Eridanus supergroup. Galaxies from the 2MASS All-Sky XSC are shown as the grey dots. Putative UDGs and H I detected LSB dwarf are shown as the green squares and the blue triangle, respectively. The red dots represent the SMUDGes UDG candidates in the Eridanus field. The black circles mark the maximum radial extents of each subgroup. The WALLABY footprint is $\sim 6° \times 6°$, which is shown as the dashed diamond.

The centroid of the NGC 1332 group is 43 kpc from the brightest lenticular galaxy (NGC 1332). It lacks X-ray emission because it is not hot enough in a low-density environment and as a virialized low-mass group. It is also not as dynamically mature as the NGC 1407 group (Brough et al. 2006). The formation of UDGs is possibly ongoing in the NGC 1332 and Eridanus groups. If satellite accretion is one of the formation mechanisms for UDGs to exist in the Eridanus supergroup, it might explain why the mature group has fewer UDG candidates to begin with as they might have been disrupted or merged into the central galaxy. Further simulations might shed some light on the number of UDGs in various evolutionary stages of galaxy group. There are also only a few foreground galaxies (based on spectroscopic redshift) within the Eridanus field. Their large projected distances with our putative UDGs would make them unlikely to be the host galaxy.

3.4 Tidal or ram-pressure stripping

Comparison of UDGs in the NIHAO simulations and in the simulation of a galaxy group (Jiang et al. 2019) shows that satellite UDGs are mostly quiescent and gas-poor. In this scenario, satellite UDGs are presumably puffed up in the field and later quenched when falling into a dense environment. The main quenching mechanisms in galaxy groups are tidal and/or ram-pressure stripping. If the tidal mechanism is dominant, the gas will be stripped and the stars will be removed from the outskirts of the satellite UDGs, which reduces their r_{eff} and M_*. We would also expect M_* to be lower for UDGs closer to the group centre due to stronger tidal effects. The studies of UDGs in HCGs (Román & Trujillo 2017b) and in the Coma cluster (Alabi et al. 2018) support this scenario, with red UDGs predominantly located closer to the group and cluster centres.

In general, the NIHAO simulation is consistent with the observations of UDGs being quiescent (red) in the inner part of the galaxy
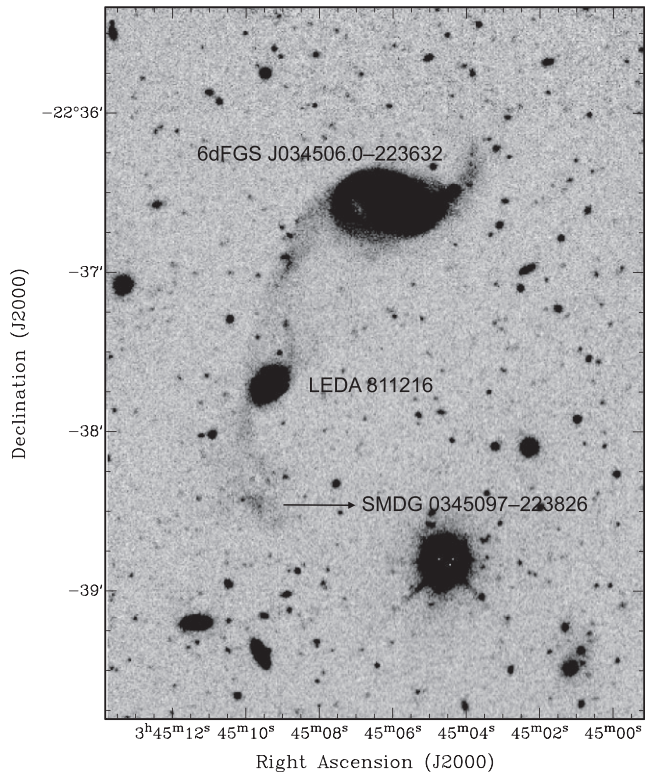
Figure 8. Co-added *g*-band image from the DR9 imaging Legacy Surveys. The locations of 6dFGS J034506.0−22363, LEDA 811216, and SMDG 0345097−223826 are labelled.

groups and star-forming (bluer) toward the outskirts of the galaxy groups. However, simulations do not show an obvious radial gradient in size or stellar mass, which suggests that tidal stripping might not be the dominant mechanism in quenching the UDGs in groups (Jiang et al. 2019). Following the evolutionary paths of satellite UDGs in simulations, Jiang et al. (2019) show that tidally induced puffing is only partially responsible for the lack of radial extent, and the change in stellar mass is small. While the sample is small, our study with the five putative UDGs in the Eridanus group neither show colour nor stellar mass versus projected distance correlations. There are no such correlations for the rest of our LSB dwarfs either, which supports the scenario of UDGs being formed via accretion in the Eridanus and NGC 1332 groups.

To investigate if our putative UDGs have experienced tidal heating, tidal or ram-pressure stripping origin, we search for any bright galaxies within 2 arcmin radius around them. While UDGs with tidal origin are generally located close (<20 kpc projected distance) to their parent galaxies (see e.g. Jones et al. 2021), they potentially form as far as 40 kpc in projected distance from their progenitors (see e.g. Iodice et al. 2020). We find that SMDG 0345097−223826 appears to be located at the tail end of a stellar stream of 6dFGS J034506.0−223632 (see Fig. 8). There is also a fairly blue spiral galaxy, LEDA 811216, that is located south of 6dFGS J034506.0−223632 and alongside the stellar stream. The location of LEDA 811216 could be a projection effect or it could in fact be interacting with 6dFGS J034506.0−22363. We retrieve the spectroscopic and photometric redshifts of 0.04249 ± 0.00015 (Jones et al. 2009) and 0.010 ± 0.006 (Zhou et al. 2021) for 6dFGS J034506.0−22363 and LEDA 811216, respectively.

The photometric redshift error is built upon with a few assumptions and using the random forest regression routine of a machine learning library, Scikit-Learn (Pedregosa et al. 2011). It is subject to the training sets and does not include incompleteness in the training data or uncertainties in morphological parameters. Luminous red galaxies are the main sample in the study of Zhou et al. (2021), which is biased toward higher redshift and redder objects. LEDA 811216 is relatively blue with $g - r = 0.34$. Hence, the quoted photometric redshift of LEDA 811216 is unlikely to be accurate.

The slight disruption on the optical morphology of LEDA 811216 suggests that this pair is interacting. We do not find any H I in any of our velocity ranges at their locations. If SMDG 0345097−223826 is associated with 6dFGS J034506.0−223632, we can rule out that it is a member of the Eridanus group. At that redshift distance, SMDG 0345097−223826 would be considered to be large in size ($r_{\mathrm{eff}} > 13$ kpc). We cannot verify the nature and origin of SMDG 0345097−223826 without follow-up spectroscopic redshift observation.

4 SUMMARY AND FUTURE WORK

We use the WALLABY pre-pilot survey data of the Eridanus field (F21) to search for H I in optically identified UDG candidates in the third release of the SMUDGes catalogue (Zaritsky et al. 2022). There are 78 UDG candidates within the maximum radial extents of the Eridanus subgroups and there is only one reliable H I detection. The detection is a confirmed member of the Eridanus group (see F21). We investigate the properties and derive the physical parameters of these SMUDGes UDG candidates. Using $r_{\mathrm{eff}} > 1.5$ kpc and $\mu_{0,\mathrm{g}} \geq 24$ mag arcsec^{-2} as the definition of a UDG, we obtain six putative UDGs. The rest is classified as LSB dwarfs. We also find that our SMUDGes UDG candidates (LSB dwarfs + putative UDGs) sample is generally low mass ($M_* < 10^8$ M$_\odot$) and most of them are fairly red in colour ($g - r > 0.45$).

It is inconclusive if our SMUDGes UDG candidates (LSB dwarfs + putative UDGs) sample yields a flattening trend at the low-mass regime while examining the $M_{\mathrm{H\,I}}/M_*$ versus M_* scaling relation. The distribution of gas richness versus colour shows no correlation in our SMUDGes UDG candidates (LSB dwarfs + putative UDGs) sample. The two putative UDGs and two LSB dwarfs that have $g - r < 0.45$ appear to have smoother optical morphology. There is no H I detection among them. This supports the finding of Karunakaran et al. (2020), which states that the optical morphology is also an important parameter when looking for H I in UDGs.

We adopt the derived power-law relation of UDG number and the virial mass of their host halo in Lee et al. (2020b) to obtain the predicted numbers of UDGs for the Eridanus subgroups. Lee et al. (2020b) predict 3, 5, and 17 for the NGC 1332, Eridanus, and NGC 1407 groups, respectively. The corresponding numbers of putative UDGs are 1^{+3}_{-1}, 5^{+8}_{-5}, and 0^{+2}. The lack of putative UDGs in the NGC 1407 group is likely due to the evolutionary stage of that group. We investigate if tidal or ram-pressure stripping is a possible formation mechanism for UDGs in the Eridanus supergroup. We find a putative UDG (SMDG 0345097−223826) that could have been formed via tidal heating/interaction as it is located at the tail end of a stellar stream. If that was the case, this putative UDG would likely be a background UDG and would not be associated with the Eridanus group.

It is known that the gas content of galaxies in the group environment is more diverse as it depends on the evolutionary stages of the group. To understand if such variation is also observed for UDGs in groups, we conduct a pilot study of H I content of SMUDGes UDG

candidates in the Eridanus supergroup using the WALLABY data in conjunction with deep optical images and catalogue. To extend what to expect for the WALLABY full survey, we cross-match the full WALLABY survey area with the third release of the SMUDGes catalogue (Zaritsky et al. 2022). We find ∼1750 SMUDGes UDG candidates within the overlapping survey area. With one H I detection out of 78 SMUDGes UDG candidates, we could expect ∼22 H I detections as the lower limit for the full WALLABY survey. There are WALLABY survey areas that are currently not covered by the DR9 DESI Legacy Survey, which is the third release of the SMUDGes catalogue based on. In addition, we expect the H I detection rate to be higher in the isolated and loose group environments. The H I redshift of isolate detections would be of great benefit as these are difficult to associate with local overdensities. In the future, this study will be expanded by using WALLABY current released pilot and full survey data, which will allow us to probe the H I content and UDG formation channels across environments.

DATA AVAILABILITY

The data underlying this article are available in the article and in its online supplementary material. The processed ASKAP data can be retrieved via CSIRO ASKAP Science Data Archive (CASDA) with a given scheduling block identification number. The DOI for the Eridanus data is https://dx.doi.org/10.25919/0yc5-f769.

REFERENCES

Abazajian K. N., et al., 2009, ApJS, 182, 543
Abraham R. G., van Dokkum P. G., 2014, PASP, 126, 55
Adams E. A. K., Oosterloo T. A., 2018, A&A, 612, A26
Alabi A. et al., 2018, MNRAS, 479, 3308
Amorisco N. C., Loeb A., 2016, MNRAS, 459, L51
Baker R. H., 1933, Ann. Harv. Coll. Obs., 88, 77
Barnes D. G. et al., 2001, MNRAS, 322, 486
Beasley M. A., Trujillo I., 2016, ApJ, 830, 23
Beasley M. A., Romanowsky A. J., Pota V., Navarro I. M., Martinez Delgado D., Neyer F., Deich A. L., 2016, ApJ, 819, L20
Bellazzini M., Belokurov V., Magrini L., Fraternali F., Testa V., Beccari G., Marchetti A., Carini R., 2017, MNRAS, 467, 3751
Bennet P., Sand D. J., Zaritsky D., Crnojević D., Spekkens K., Karunakaran A., 2018, ApJ, 866, L11
Bothun G. D., Impey C. D., Malin D. F., 1991, ApJ, 376, 404
Boylan-Kolchin M., Bullock J. S., Kaplinghat M., 2012, MNRAS, 422, 1203
Brodie J. P., Romanowsky A. J., Strader J., Forbes D. A., 2011, AJ, 142, 199
Brough S., Forbes D. A., Kilborn V. A., Couch W., Colless M., 2006, MNRAS, 369, 1351
Carleton T., Guo Y., Munshi F., Tremmel M., Wright A., 2021, MNRAS, 502, 398
Catinella B. et al., 2018, MNRAS, 476, 875
Chabrier G., 2003, PASP, 115, 763
Chilingarian I. V., Afanasiev A. V., Grishin K. A., Fabricant D., Moran S., 2019, ApJ, 884, 79
Conselice C. J., 2018, Res. Notes Am. Astron. Soc., 2, 43
da Costa L. N. et al., 1988, ApJ, 327, 544
Dalcanton J. J., Spergel D. N., Gunn J. E., Schmidt M., Schneider D. P., 1997, AJ, 114, 635
de Vaucouleurs G., 1975, in Sandage A., Sandage M., Kristian J., eds, Galaxies and the Universe. Univ. Chicago Press, Chicago, p. 557
Dey A. et al., 2019, AJ, 157, 168
Di Cintio A., Brook C. B., Dutton A. A., Macciò A. V., Obreja A., Dekel A., 2017, MNRAS, 466, L1
Eigenthaler P. et al., 2018, ApJ, 855, 142
Emsellem E. et al., 2019, A&A, 625, A76
For B.-Q. et al., 2019, MNRAS, 489, 5723
For B.-Q. et al., 2021, MNRAS, 507, 2300 (F21)
Forbes D. A., Alabi A., Romanowsky A. J., Brodie J. P., Arimoto N., 2020, MNRAS, 492, 4874
Giovanelli R. et al., 2005, AJ, 130, 2598
Habas R. et al., 2020, MNRAS, 491, 1901
Hotan A. W. et al., 2021, PASA, 38, e009
Huang S., Haynes M. P., Giovanelli R., Brinchmann J., Stierwalt S., Neff S. G., 2012, AJ, 143, 133
Impey C., Bothun G., Malin D., 1988, ApJ, 330, 634
Iodice E. et al., 2020, A&A, 642, A48
Iodice E. et al., 2021, A&A, 652, L11
Janowiecki S., Catinella B., Cortese L., Saintonge A., Brown T., Wang J., 2017, MNRAS, 466, 4795
Janowiecki S., Jones M. G., Leisman L., Webb A., 2019, MNRAS, 490, 566

Janssens S., Abraham R., Brodie J., Forbes D., Romanowsky A. J., van Dokkum P., 2017, ApJ, 839, L17

Janssens S. R. et al., 2022, MNRAS, 517, 858

Jarrett T. H., Chester T., Cutri R., Schneider S., Skrutskie M., Huchra J. P., 2000, AJ, 119, 2498

Jiang F., Dekel A., Freundlich J., Romanowsky A. J., Dutton A. A., Macciò A. V., Di Cintio A., 2019, MNRAS, 487, 5272

Johnston S. et al., 2007, PASA, 24, 174

Jones D. H. et al., 2004, MNRAS, 355, 747

Jones D. H. et al., 2009, MNRAS, 399, 683

Jones M. G., Bennet P., Mutlu-Pakdil B., Sand D. J., Spekkens K., Crnojević D., Karunakaran A., Zaritsky D., 2021, ApJ, 919, 72

Junais et al., 2022, A&A, 667, A76

Kado-Fong E., Greene J. E., Huang S., Goulding A., 2022, ApJ, 941, 11

Kadowaki J., Zaritsky D., Donnerstein R. L., 2017, ApJ, 838, L21

Kadowaki J., Zaritsky D., Donnerstein R. L., RS P., Karunakaran A., Spekkens K., 2021, ApJ, 923, 257

Karunakaran A., Zaritsky D., 2023, MNRAS, 519, 884

Karunakaran A., Spekkens K., Zaritsky D., Donnerstein R. L., Kadowaki J., Dey A., 2020, ApJ, 902, 39

Kleiner D. et al., 2019, MNRAS, 488, 5352

Koda J., Yagi M., Yamanoi H., Komiyama Y., 2015, ApJ, 807, L2

Koribalski B. S. et al., 2020, Ap&SS, 365, 118

Lee M. G., Kang J., Lee J. H., Jang I. S., 2017, ApJ, 844, 157

Lee C. H., Hodges-Kluck E., Gallo E., 2020a, MNRAS, 497, 2759

Lee J. H., Kang J., Lee M. G., Jang I. S., 2020b, ApJ, 894, 75

Leisman L. et al., 2017, ApJ, 842, 133

Lim S. et al., 2020, ApJ, 899, 69

McQuinn K. B. W. et al., 2021, ApJ, 918, 23

Maddox N., Hess K. M., Obreschkow D., Jarvis M. J., Blyth S.-L., 2015, MNRAS, 447, 1610

Mancera Piña P. E., Peletier R. F., Aguerri J. A. L., Venhola A., Trager S., Choque Challapa N., 2018, MNRAS, 481, 4381

Mancera Piña P. E. et al., 2020, MNRAS, 495, 3636

Marleau F. R. et al., 2021, A&A, 654, A105

Martin G. et al., 2019, MNRAS, 485, 796

Martín-Navarro I. et al., 2019, MNRAS, 484, 3425

Merritt A., van Dokkum P., Danieli S., Abraham R., Zhang J., Karachentsev I. D., Makarova L. N., 2016, ApJ, 833, 168

Mihos J. C. et al., 2015, ApJ, 809, L21

Miles T. A., Raychaudhury S., Forbes D. A., Goudfrooij P., Ponman T. J., Kozhurina-Platais V., 2004, MNRAS, 355, 785

Murugeshan C. et al., 2021, MNRAS, 507, 2949

Omar A., Dwarakanath K. S., 2005, J. Astrophys. Astron., 26, 1

Papastergis E., Adams E. A. K., Romanowsky A. J., 2017, A&A, 601, L10

Pedregosa F. et al., 2011, J. Mach. Learn. Res., 12, 2825

Prole D. J., van der Burg R. F. J., Hilker M., Davies J. I., 2019, MNRAS, 488, 2143

Prole D. J., van der Burg R. F. J., Hilker M., Spitler L. R., 2021, MNRAS, 500, 2049

Román J., Trujillo I., 2017a, MNRAS, 468, 703

Román J., Trujillo I., 2017b, MNRAS, 468, 4039

Román J., Jones M. G., Montes M., Verdes-Montenegro L., Garrido J., Sánchez S., 2021, A&A, 649, L14

Rong Y., Guo Q., Gao L., Liao S., Xie L., Puzia T. H., Sun S., Pan J., 2017, MNRAS, 470, 4231

Ruiz-Lara T. et al., 2018, MNRAS, 478, 2034

Saintonge A., Catinella B., 2022, ARA&A, 60, 319

Sawala T. et al., 2016, MNRAS, 457, 1931

Scott T. C., Sengupta C., Lagos P., Chung A., Wong O. I., 2021, MNRAS, 503, 3953

Serra P. et al., 2015, MNRAS, 448, 1922

Shi D. D. et al., 2017, ApJ, 846, 26

Spekkens K., Karunakaran A., 2018, ApJ, 855, 28

Spergel D. N. et al., 2007, ApJS, 170, 377

Tran K.-V. H., Saintonge A., Moustakas J., Bai L., Gonzalez A. H., Holden B. P., Zaritsky D., Kautsch S. J., 2009, ApJ, 705, 809

van der Burg R. F. J., Muzzin A., Hoekstra H., 2016, A&A, 590, A20

van der Burg R. F. J. et al., 2017, A&A, 607, A79

van Dokkum P. G., Abraham R., Merritt A., Zhang J., Geha M., Conroy C., 2015, ApJ, 798, L45

Venhola A. et al., 2017, A&A, 608, A142

Wang L., Dutton A. A., Stinson G. S., Macciò A. V., Penzo C., Kang X., Keller B. W., Wadsley J., 2015, MNRAS, 454, 83

Wang S. et al., 2022, ApJ, 927, 66

Westmeier T. et al., 2021, MNRAS, 506, 3962

Willmer C. N. A., 2018, ApJS, 236, 47

Willmer C. N. A., Focardi P., da Costa L. N., Pellegrini P. S., 1989, AJ, 98, 1531

Wolfinger K., Kilborn V. A., Ryan-Weber E. V., Koribalski B. S., 2016, Publ. Astron. Soc. Aust., 33, e038

Wong O. I. et al., 2021, MNRAS, 507, 2905

Wright A. C., Tremmel M., Brooks A. M., Munshi F., Nagai D., Sharma R. S., Quinn T. R., 2021, MNRAS, 502, 5370

Yagi M., Koda J., Komiyama Y., Yamanoi H., 2016, ApJS, 225, 11

Yozin C., Bekki K., 2015, MNRAS, 452, 937

Zaritsky D., 2017, MNRAS, 464, 110

Zaritsky D. et al., 2019, ApJS, 240, 1

Zaritsky D., Donnerstein R., Karunakaran A., Barbosa C. E., Dey A., Kadowaki J., Spekkens K., Zhang H., 2021, ApJS, 257, 60

Zaritsky D., Donnerstein R., Karunakaran A., Barbosa C. E., Dey A., Kadowaki J., Spekkens K., Zhang H., 2022, ApJS, 261, 11

Zhou R. et al., 2021, MNRAS, 501, 3309

Zibetti S., Charlot S., Rix H.-W., 2009, MNRAS, 400, 1181

SUPPORTING INFORMATION

Supplementary data are available at *MNRAS* online.

Additional supporting information can be found in the online version of this article.

Table 1: Properties and derived parameters of selected SMUDGes sample.

Please note: Oxford University Press is not responsible for the content or functionality of any supporting materials supplied by the authors. Any queries (other than missing material) should be directed to the corresponding author for the article.

This paper has been typeset from a TeX/LaTeX file prepared by the author.